Frequency locking and the loss of spatial coherence for driven space-charge domains in ultrapure Ge

A. M. Kahn,* D. J. Mar, and R. M. Westervelt

Division of Applied Sciences, Harvard University, Cambridge, Massachusetts 02138
and Department of Physics, Harvard University, Cambridge, Massachusetts 02138

(Received 18 December 1991)

Spatially resolved measurements of the dynamics of sinusoidally driven space-charge domains in ultrapure Ge are presented for frequency-locked and driven chaotic oscillations. At liquid-He temperatures, moving space-charge domains form due to impact ionization of shallow acceptors, resulting in a spontaneous periodic current oscillation for dc voltage bias. With a superimposed sinusoidal ac voltage bias, these oscillations exhibit frequency locking and a quasiperiodic transition to chaos similar to those studied previously in the time domain by Gwinn and Westervelt. Spatial measurements using an array of capacitive probes show that frequency locking and the transition to chaos initially occur via modulation of the amplitude and motion of a single domain; thus the dynamics can be described by a low-dimensional model. For larger ac drives in the chaotic region above the critical line, spatial coherence is lost as domains form and disappear in the interior of the sample, and the electric field profile becomes spatially complex.

I. INTRODUCTION

Bulk instabilities at low temperatures ($T < 30$ K) are observed in a number of semiconductors including Ge,[1-4] GaAs,[5] InSb,[6] and Si.[7] These instabilities typically occur due to a regime of negative differential conductivity (NDC), as suggested by Ridley.[8] In cooled ultrapure Ge, a spontaneous current oscillation occurs beyond the threshold for impurity breakdown due to a region of carrier-concentration-based NDC resulting from impact ionization of shallow acceptors.[9-11] We have recently used a movable capacitive probe to show that each period of this current oscillation is due to the nucleation and passage of a high-field domain through the sample.[12] Because the domain is composed of trapped space charge, the domain velocity is much slower than the free-carrier drift velocity.[12]

The temporal frequency-locking behavior for the oscillation in Ge with added sinusoidal drive has been studied in detail in the temporal regime by Gwinn and Westervelt.[4,13] These authors found quantitative agreement between the quasiperiodic transition to chaos observed in Ge and universal predictions of the circle map.[4,13] The corresponding high-field domain motion in Ge during the quasiperiodic transition to chaos was not studied in this earlier work, and interesting questions remain open: When the current becomes chaotic, do the variations in the sample electric field remain spatially coherent, or do they become more complex? Held and Jeffries investigated the loss of spatial coherence for a nondriven helical instability[14] in an electron-hole plasma in n-type Ge at 77 K. Recently, Mosekilde et al. have reported evidence for complex spatial structures in numerical simulations of driven chaotic Gunn diodes.[15]

In this paper we present time-resolved spatial measurements of electric field profiles of space-charge domains in ultrapure Ge when the sample oscillation is frequency locked and driven into the chaotic regime with a sinusoidal ac voltage added to a dc voltage bias. We use an array of capacitive probes to measure the spatially dependent electric field $E(x,t)$ associated with the driven instability. In the absence of an ac drive, each period of the spontaneous oscillation has been previously shown[12] to be due to a single space-charge domain transversing the sample. In the frequency-locked regime below the critical line, the spatial structure remains simple: a single domain is present, but its height and velocity are modulated by the external drive. As the drive amplitude is increased into the chaotic regime, the spatial structure is at first coherent, composed of a single domain modulated chaotically in height and velocity. This result is consistent with earlier temporal measurements of the quasiperiodic transition to chaos in this system by Gwinn and Westervelt,[4,13] which were in quantitative agreement with the circle map, a low-dimensional model. As the drive amplitude is increased further into the chaotic regime, we observe both a gradual loss of spatial coherence and higher-dimensional behavior due to the nucleation and destruction of high-field domains in the interior of the sample. An early account of some of this work has been reported in Ref. 16.

In theory, it may be possible to predict the drive parameters for which spatial coherence is lost by determining when domains nucleate and decay in the bulk of the sample. However, this problem is difficult because different parts of the sample are coupled by the requirement that the integral of the electric field along the sample equal the applied voltage. Hence, the growth of a high-field domain in one part of the sample reduces the electric field in other locations, and may suppress the growth of domains or destroy existing domains, leading to complex spatiotemporal dynamics. Criteria for the nucleation and destruction of domains inside the sample are determined in part by the local time-dependent profiles of electric field and trapped charge density. For example, if the electric field profile within a region is approximately

homogeneous with an average value greater than E_c, the threshold for spontaneous periodic current oscillations, then it is likely that a high-field domain will be nucleated within that region. Also, if the local trapped charge density is high, then a domain is more likely to form because the net rate of impact ionization is increased.

The organization of this paper is as follows: Section II presents experimental information and definitions. In Sec. III we discuss the temporal behavior of the current and the corresponding electric field profiles for frequency-locked oscillations. Section IV shows data for a driven chaotic oscillation which displays spatially coherent behavior. Section V presents data for a driven chaotic oscillation with larger drive amplitude, for which the electric field profiles are much more complicated and a loss of spatial coherence is observed. In Section VI we explore the effect of the bias voltage, the drive amplitude, and the drive frequency on the spatial coherence. Section VII presents our conclusions.

II. EXPERIMENTAL PROCEDURES

The sample used for these measurements was cut from a crystal of undislocated p-type ultrapure Ge with residual shallow acceptor concentration $N_A \sim 1 \times 10^{11}$ cm^{-3}, grown by E. E. Haller and associates at Lawrence Berkeley Laboratory; the sample characteristics are described in detail in Ref. 12. Samples from the same crystal were used in earlier work on frequency-locking by Gwinn and Westervelt.[4,13] Similar behavior is also found for samples cut from other crystals with comparable shallow acceptor concentrations but with dislocations.[17] We have experimentally verified the absence of current filaments,[17] which are observed in doped Ge with much higher impurity concentrations.[18] After cutting to size $14.5 \times 4.0 \times 4.0$ mm^3 and etching to remove surface damage, Ohmic contacts were fabricated across opposing 4×4 mm^2 faces via boron ion implantation. This produces a thin, degenerately doped p^+ layer which acts as a reservoir for holes in p-type Ge at liquid-He temperatures. This geometry is chosen to ensure that electric field lines lie primarily along the length of the sample. The sample is mounted atop an array of capacitive probes as described below, and cooled to liquid-He temperatures by immersion in a cryostat. The temperature is held at 4.2 K by maintaining the liquid He at atmospheric pressure, and the sample is surrounded by a cold radiation shield held at the same temperature.

The voltage profile along the sample is measured with an array of 16 capacitive probes fabricated using optical lithography on a sapphire substrate. Each probe is 300 μm wide and extends across the entire width of the sample, perpendicular to the conduction direction. The probes are arranged in eight pairs equally spaced along the 14.5-mm length of the sample, which is insulated by a thin (50-μm) sheet of mica. The capacitance of each probe to the sample is calibrated by applying an ac drive superimposed upon a dc voltage bias in the postbreakdown regime, but well below the threshold E_c; the probe-to-sample capacitance is ≈ 0.2 pF. An array of 16 charge-coupled amplifiers is used to sense the sample

voltage profile, and the outputs of these amplifiers are simultaneously digitized at a rate of 50 kHz per probe using a 16-channel A/D converter. The undesirable effects of probe-to-ground capacitance and coupling between probes are minimized by maintaining the probes at virtual ground. Because the probe-to-sample capacitance is small, perturbation of space-charge domain motion by the probes is negligible. The electric field profile is obtained by subtracting the sample voltages at each pair of probes. The spatial resolution for this measurement is approximately 400 μm, the center-to-center distance between probes.

The samples are voltage biased with a sinusoidal ac drive voltage superimposed upon a dc voltage so that the total applied electric field (equal to the applied voltage divided by the sample length) E_{total} is given by

$$E_{\text{total}}(t) = E_{\text{dc}} + A \sin(2\pi f_d t) , \qquad (1)$$

where E_{dc} is the dc part of the applied field, A is the drive amplitude, and f_d is the drive frequency. By analogy with circle-map theory,[19] the frequency is expressed in terms of the ratio f_0/f_d, where f_0 is the fundamental oscillation frequency for dc bias. The sample current is obtained by measuring the voltage across a small (10 Ω) series resistor. For all results reported in this paper, except as specified in Sec. VI, the dc part of the applied electric field is fixed at $E_{\text{dc}} = 7.45$ V/cm, which is above the threshold $E_c = 6.3$ V/cm for spontaneous periodic current oscillations. The fundamental frequency f_0 of the spontaneous periodic oscillation for this dc bias field is 1.2 kHz.

In order to understand the effect of the ac drive on the spatial coherence, we measure the spatially dependent electric field $E(x,t)$ associated with a range of drive parameters. As a measure of the spatial coherence, we use the linear correlation coefficient $r_t(x,\tau)$, defined as[20]

$$r_t(x,\tau) = \frac{\left[\sum_d E(d,t)E(d-x,t+\tau) \right]}{\left[\sum_d E(d,t)^2 \sum_d E(d-x,t+\tau)^2 \right]^{1/2}} , \qquad (2)$$

where x and d are discrete distances along the conduction direction and τ is a time interval measured from an initial time t. This function is sensitive only to changes in the shape of the electric field profile, because the normalization in the denominator removes the effects of differences in the overall amplitude of the signals. Thus, $r_t(x,\tau) = 1$ corresponds to correlated motion, $r_t(x,\tau) = 0$ corresponds to uncorrelated motion, and $r_t(x,\tau) = -1$ corresponds to anticorrelated motion. For each set of drive parameters, we record the spatially dependent electric field for 40 ms, and then calculate $r_t(x,\tau)$ using 1000 different values of t, separated by 40 μs. We then average over t to determine $r(x,\tau)$:

$$r(x,\tau) = \langle r_t(x,\tau) \rangle_t . \qquad (3)$$

The function $r(x,\tau)$ is peaked at a time for a domain to move a distance x.

III. FREQUENCY-LOCKING DATA

This section presents data for the current and the electric field profiles associated with frequency-locked oscillations. Frequency locking was studied in the temporal domain using similar samples by Gwinn and Westervelt.[4] In this section we consider only relatively small applied ac drive amplitudes, so that the domain motion remains spatially coherent. In Sec. V, we examine the case when the drive amplitude A is sufficiently large that domains are created and destroyed inside the sample and domain motion is spatially incoherent.

The temporal behavior of the driven oscillation in the frequency-locked regime is summarized by the Arnold tongue diagram in drive parameter space. Figure 2 of Ref. 16 shows a series of Arnold tongues, within each of which the sample oscillation is locked onto the drive in a simple rational ratio. Experimentally, each tongue is mapped by varying the frequency of the applied drive and determining when the oscillation becomes unlocked using a spectrum analyzer. The tongues extend vertically for increasing drive amplitude until hysteresis is first observed in the boundary of the tongue as the drive frequency is varied. Even though this is a spatially extended system, it has been shown to be well described at the quasiperiodic transition to chaos by the circle map,[4,13] which is a low-dimensional model. In this model, hysteresis in the boundaries of the Arnold tongues is identified with the critical line. The tops of the Arnold tongues approximate the critical line, which is not necessarily a smooth curve. Above the critical line, the tongues overlap and it is possible to drive the oscillation chaotic.

Figure 1 shows the temporal and spatial behavior for a frequency-locked oscillation with a 1:1 locking. The applied ac drive shown in Fig. 1(a) has amplitude $A = 0.78$ V/cm and drive ratio $f_0/f_d = 1.00$, above the critical line in Fig. 2 of Ref. 16. The ac part of the resulting current oscillation is plotted in Fig. 1(b) using the same time scale as in Fig. 1(a). The oscillation has a shape very similar to that observed for the spontaneous periodic current oscillation,[12] with a sharp decrease in current followed by a slower increase. The spatially dependent electric field $E(x,t)$ measured with the array of capacitive probes is shown in Fig. 1(c). The local electric field as a function of time is shown at eight equally spaced positions along the sample with the trace taken closest to the injecting contact at the bottom of the figure. As shown, a high-field domain nucleates at the injecting contact and moves smoothly through the sample. The domain appears similar to those observed in Ref. 12 for the spontaneous current oscillation. As the domain in Fig. 1(c) approaches the receiving contact, the domain amplitude decreases and a new domain is nucleated at the injecting contact.

Figure 2 shows results for a 1:2 locking of the current oscillation to the added ac drive. The drive parameters are $A = 0.78$ V/cm (as used for Fig. 1) and $f_0/f_d = 0.48$. The ac part of the applied bias is shown in Fig. 2(a) and the ac part of the current is shown in Fig. 2(b). The current oscillation appears similar to the current oscillation for the 1:1 locking shown in Fig. 1(b), except that the
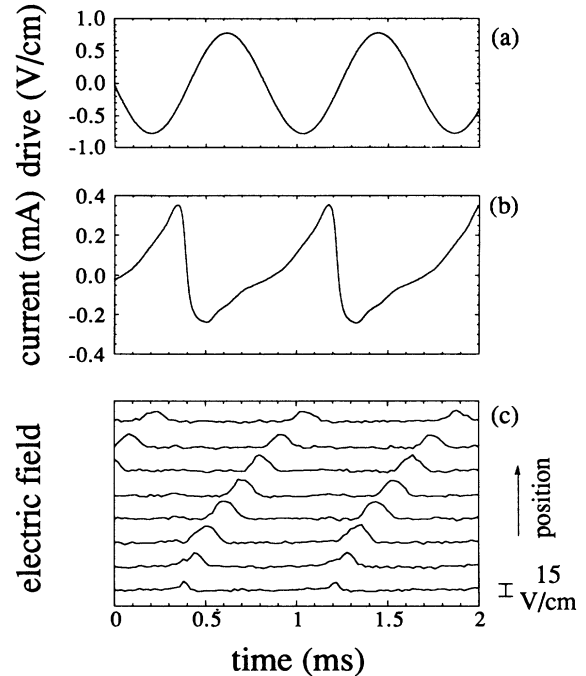

FIG. 1. Data taken for a 1:1 locking of the current oscillation onto the added ac drive, with $E_{dc} = 7.45$ V/cm, $A = 0.78$ V/cm, and $f_0/f_d = 1.00$: (a) Time-dependent part of $E_{total}(t)$; (b) time-dependent part of the sample current; (c) local sample electric field vs time at eight equally spaced locations with the trace nearest the injecting contact at the bottom. The time axes are the same in (a)–(c).

oscillation shown in Fig. 2(b) has an additional feature on the rising portion of the current trace. Figure 2(c) shows the corresponding electric field as a function of time at successive positions. The figure shows a moving space-charge domain periodically traversing the sample as in Fig. 1(c). The period of the domain motion in Fig. 2(c) does not correspond to the drive period, but rather to the slower fundamental period of the oscillation. The drive frequency is manifested in the measured sample electric field as a modulation in the amplitude and velocity of the domain as it moves through the sample.

The phase of the domain motion in Figs. 1(c) and 2(c) is such that each new domain is nucleated on the rising edge of the ac drive. In general for this system, the observed behavior of lockings which are of the form 1:N, where N is an integer, is analogous to the 1:2 locking shown in Fig. 2. Every N drive cycles, a domain is nucleated at the injecting contact on the rising edge of the drive. The amplitude and velocity of the domain are modulated by the drive as the domain moves through the sample. Lockings which are not of the form 1:N involve the nucleation of domains on more than one phase of the ac drive. For these lockings, we observe domains nucleated on the falling edge of the drive as well as the rising edge. The domains nucleated on the falling edge start in the bulk of the sample, away from the injecting contact.

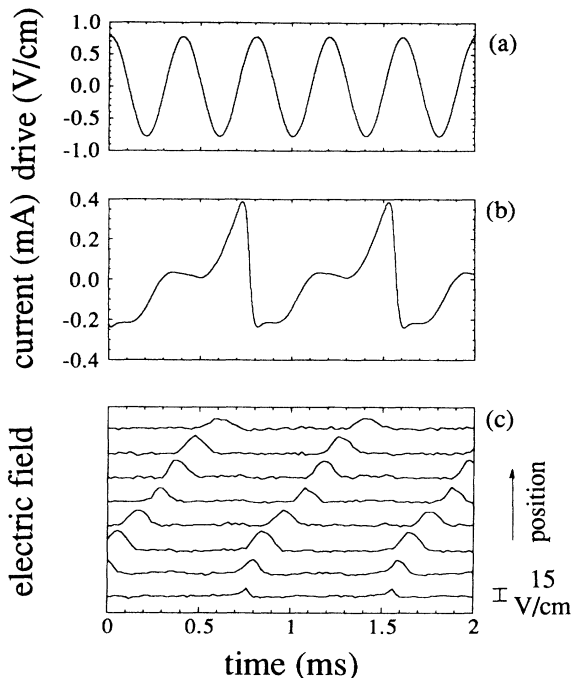Figure 3 shows data taken for a 2:3 locking of the sample oscillation to the external drive, with drive parame-

FIG. 2. Data taken for a 1:2 locking of the current oscillation onto the added ac drive, with $E_{dc} = 7.45$ V/cm, $A = 0.78$ V/cm, and $f_0/f_d = 0.48$: (a) Time-dependent part of $E_{total}(t)$; (b) time-dependent part of the sample current; (c) local sample electric field vs time at eight equally spaced locations with the trace nearest the injecting contact at the bottom. The time axes are the same in (a)–(c).

FIG. 3. Data taken for a 2:3 locking of the current oscillation onto the added ac drive, with $E_{dc} = 7.45$ V/cm, $A = 0.99$ V/cm, and $f_0/f_d = 0.68$: (a) Time-dependent part of $E_{total}(t)$; (b) time-dependent part of the sample current; (c) local sample electric field vs time at eight equally spaced locations with the trace nearest the injecting contact at the bottom. The time axes are the same in (a)–(c).

ters $A = 0.99$ V/cm and $f_0/f_d = 0.68$. The ac part of $E_{total}(t)$ is shown in Fig. 3(a) and the sample current is shown in Fig. 3(b). Because the locking is not of the form 1:N, the period of the frequency-locked oscillation is longer than the period of the fundamental oscillation; in this case the period is twice the period of the fundamental oscillation. The current oscillation has a sawtooth shape which alternates between two excursions. Figure 3(c) shows the electric-field profiles $E(x,t)$ associated with this current oscillation. The data show that the deeper excursion of the current is associated with the launching of a high-field domain at the injecting contact. This domain is nucleated on the rising edge of the ac drive, as in Figs. 1 and 2. The smaller downward excursion of the current in Fig. 3(b) is associated with the launching of a high-field domain several millimeters from the injecting contact, as shown in Fig. 3(c). Comparison with Fig. 3(a) shows that this domain is launched on the falling portion of the ac drive.

Lockings which are not of the form 1:N, for which domains nucleate at more than one drive phase, are observed to be more sensitive to changes in the drive frequency than 1:N lockings, for which all domains nucleate on the same drive phase. Hence, the Arnold tongues for the lockings which are not of the form 1:N are narrower relative to the 1:N tongues[16] than the corresponding tongues in the case of the circle map.[19] For example, the ratio of the width of the 2:3 tongue to that of the 1:2 tongue in Fig. 2 of Ref. 16 is much smaller than the corresponding ratio for the circle map.
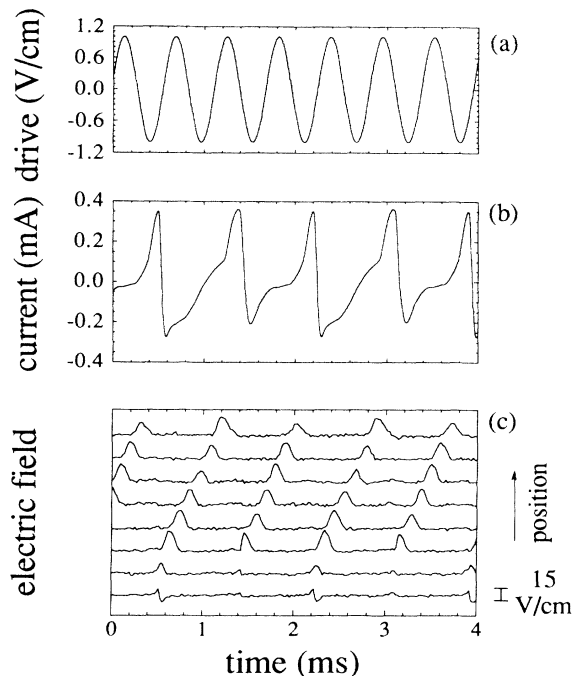
IV. TEMPORAL CHAOS, SPATIAL COHERENCE

This section presents an example of a driven chaotic oscillation for which the electric field in the sample is spatially coherent even though the current is temporally chaotic. We first discuss the temporal behavior of the driven oscillation, as measured from the sample current. Several standard techniques are used for plotting this chaotic signal. To provide contrast and to show that the nonperiodic oscillation is not due to noise, these plots of the chaotic current oscillation are juxtaposed with plots of a frequency-locked oscillation. The drive amplitude used to drive the sample oscillation chaotic is $A = 0.85$ V/cm, well above the critical line. The drive frequency is at $f_0/f_d = 0.62$, approximately equal to the golden mean $\sigma_g = (\sqrt{5}-1)/2$. Each plot of the temporal behavior is preceded by the corresponding plot for the frequency-locked oscillation at the nearest wide Arnold tongue, the 1:2 tongue. The drive parameters used for this frequency-locked data are identical to those used for Fig. 2, $A = 0.78$ V/cm and $f_0/f_d = 0.48$.

Figure 4 shows the power spectrum of the current, measured with a signal analyzer using a Hanning window, for the frequency-locked and chaotic cases. The power spectrum of the 1:2 frequency-locked oscillation, shown in Fig. 4(a), is very clean with a signal-to-noise ratio of approximately 65 dB. Figure 4(b) shows the power spectrum of the current oscillation driven chaotic with f_0/f_d approximately equal to the golden mean σ_g, plot-
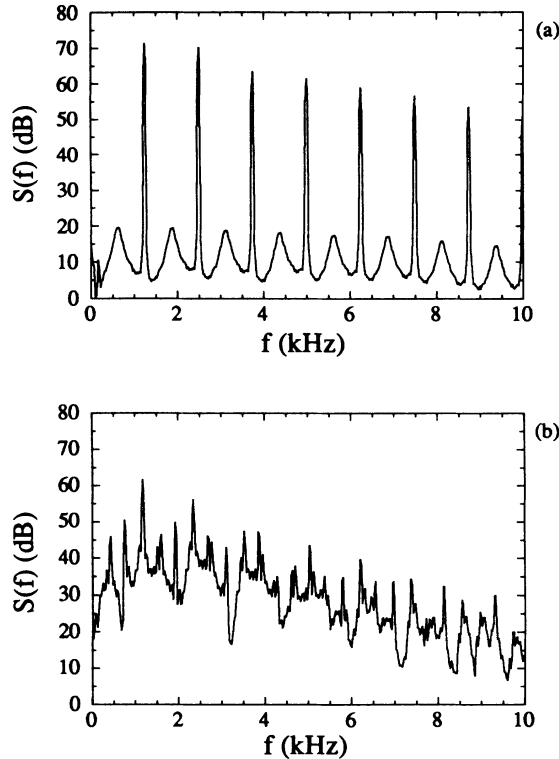
FIG. 4. Power spectra with $E_{dc}=7.45$ V/cm and (a) the oscillation locked to the drive with parameters $A=0.78$ V/cm and $f_0/f_d=0.48$; (b) the oscillation driven chaotic with drive parameters $A=0.85$ V/cm and $f_0/f_d=0.62$.

ted with the same scale as Fig. 4(a). Compared to Fig. 4(a), in Fig. 4(b) there is a large rise in the broadband noise level, as is characteristic of a chaotic oscillation.

In Fig. 5 we show the result of using the method of time delays[21] to plot the attractors using the sample current for the 1:2 frequency-locked oscillation and for the driven chaotic oscillation. In both cases the time delay $\tau=36$ μs, approximately 7% of the drive period for the driven chaotic oscillation. The reconstructed attractor for the frequency-locked oscillation is shown in Fig. 5(a). The attractor is a closed loop, as expected for a periodic oscillation. Note that the figure shows many periods of the oscillation, but because the oscillation is clean and periodic, the attractor appears as a single loop. Figure 5(b) shows the reconstructed attractor for the driven chaotic oscillation. In this case the attractor is more complicated, as expected for a chaotic attractor.

Figure 6 shows the corresponding Poincaré maps for these two oscillations. These plots are constructed by sampling the current at a fixed drive phase φ. We then construct the first return map by plotting the current at the $(n+1)$th drive cycle as a function of the current at the nth drive cycle. The Poincaré map for the 1:2 locked oscillation consists of two points because the oscillation repeats every two drive cycles. This is shown in Fig. 6(a), where for clarity we have plotted circles instead of points. The Poincaré map for the driven chaotic oscillation is shown in Fig. 6(b). The folds in the Poincaré map at the bottom and along the right in Fig. 6(b) are characteristic

of the wrinkled torus for the quasiperiodic transition to low-dimensional chaos.

The spatially dependent electric field associated with the chaotic sample oscillation is shown in Fig. 7(a). As above, the local electric field as a function of time is shown at eight equally spaced positions along the sample with the trace closest to the injecting contact at the bottom. The data show that even though the current is temporally chaotic, the electric field variations are spatially coherent in the following senses. High-field domains are observed to nucleate near the injecting contact and move smoothly through the sample. Domains are nucleated only near the injecting contact and always succeed in reaching the receiving contact. A new domain is nucleated only when the previous domain exits the sample at the receiving contact. The nonperiodic nature of the oscillation is manifested as a variation in the amplitude of the domains when they first enter the sample and as a variation in the times between domains. The observed spatial coherence beyond the quasiperiodic transition to chaos indicates that the time dependence of the driven current oscillation may be determined by only a few degrees of freedom, in agreement with Gwinn and Westervelt.[4,13]
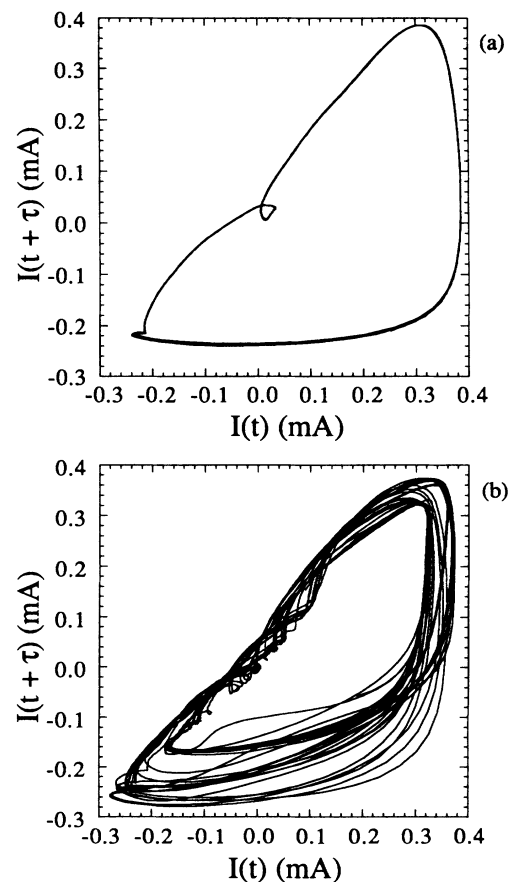

FIG. 5. Reconstructed attractors from sample current using $\tau=36$ μs with $E_{dc}=7.45$ V/cm and (a) the oscillation locked to the drive with parameters $A=0.78$ V/cm and $f_0/f_d=0.48$; (b) the oscillation driven chaotic with drive parameters $A=0.85$ V/cm and $f_0/f_d=0.62$.
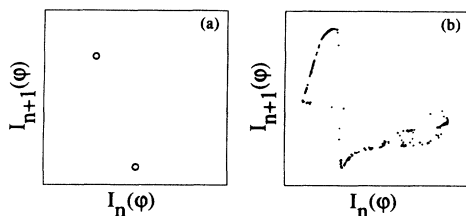
FIG. 6. Poincaré maps constructed by strobing the sample current at a fixed phase of the ac drive and plotting as a map, with $E_{dc} = 7.45$ V/cm and (a) the oscillation locked to the drive with parameters $A = 0.78$ V/cm and $f_0/f_d = 0.48$; (b) the oscillation driven chaotic with drive parameters $A = 0.85$ V/cm and $f_0/f_d = 0.62$.

Figure 7(b) shows the correlation function $r(x = 1.6$ mm,$\tau)$ as defined in Sec. II, calculated for this driven chaotic oscillation. There is a large peak in the correlation function at a time interval $\tau = 0.08$ ms. This large peak occurs because the electric field is spatially coherent. The time at which the peak occurs corresponds to the transit time for the domain to travel $x = 1.6$ mm, the distance between adjacent pairs of capacitive probes. The second peak in the correlation function occurs approximately one fundamental period later. As expected, this second peak is smaller than the first peak. A series of successively smaller peaks is observed [but not shown in Fig. 7(b)] separated by approximately one fundamental period.
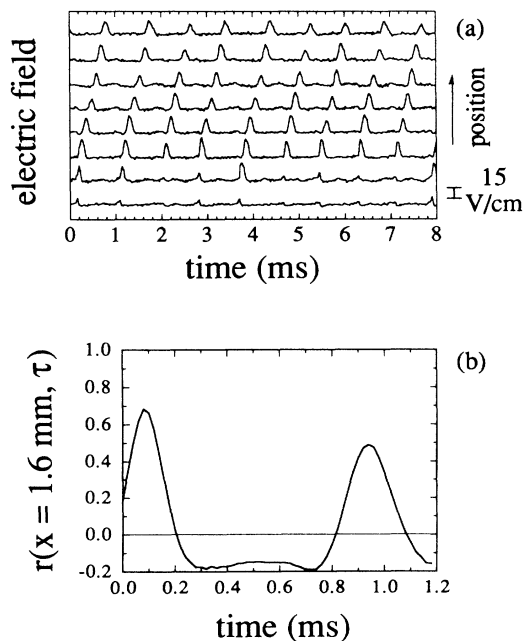
V. TEMPORAL CHAOS, SPATIAL INCOHERENCE

In Sec. IV we showed that we can drive the sample oscillation temporally chaotic while maintaining spatial coherence in the sample electric field. In this section we show that for a larger drive amplitude and higher drive frequency, the driven chaotic sample oscillation is associated with spatially incoherent variations in the sample electric field. This section is structured very similarly to Sec. IV. First, we present several different plots of the temporally chaotic sample current. Each of these is juxtaposed with the corresponding plot for a frequency-locked oscillation. The parameters used here to drive the oscillation chaotic are $A = 1.91$ V/cm and $f_0/f_d = 0.18$. This drive has a higher frequency and a larger amplitude than that used for the driven chaotic oscillation discussed in Sec. IV. The parameters used for the frequency-locked data shown in this section are $A = 1.63$ V/cm and $f_0/f_d = 0.19$, resulting in a 1:4 locking. Both of these drive amplitudes are well above the critical line.

The power spectra of the sample current are shown in Fig. 8 for each of these two sets of drive parameters. Figure 8(a) shows the power spectrum of the 1:4 locked oscillation, showing a very high signal-to-noise ratio. The power spectrum of the driven chaotic oscillation is shown in Fig. 8(b). The large sharp peak at 6.6 kHz corresponds to the strong ac drive. At lower frequencies the noise level has risen to the point where no sharp peaks can be discerned.
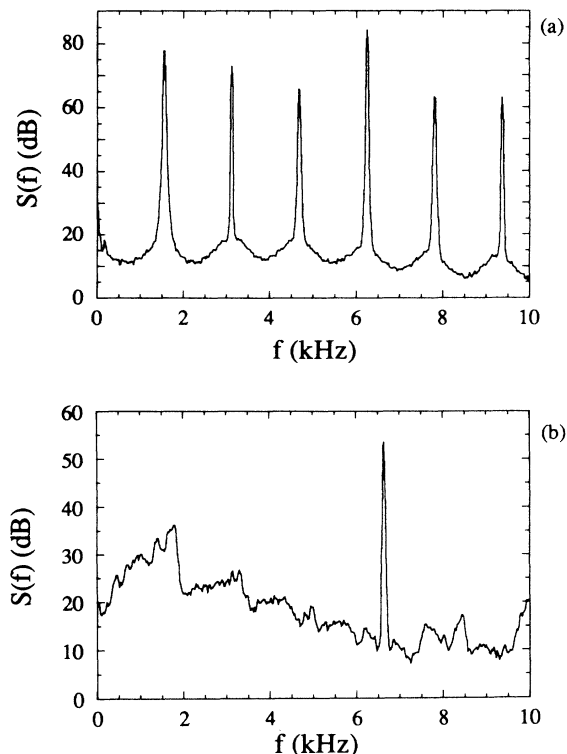

FIG. 7. Driven chaotic oscillation with $E_{dc} = 7.45$ V/cm, $A = 0.85$ V/cm, and $f_0/f_d = 0.62$: (a) local sample electric field vs time at eight equally spaced locations with the trace nearest the injecting contact at the bottom; (b) $r(x = 1.6$ mm,$\tau)$ vs τ. The horizontal line indicates $r(x = 1.6$ mm,$\tau) = 0$.

FIG. 8. Power spectra with $E_{dc} = 7.45$ V/cm and (a) the oscillation locked to the drive with parameters $A = 1.63$ V/cm and $f_0/f_d = 0.19$; (b) the oscillation driven chaotic with drive parameters $A = 1.91$ V/cm and $f_0/f_d = 0.18$.

The reconstructured attractors for these driven oscilla-
tions are shown in Fig. 9. The reconstructed attractor for
the 1:4 locked oscillation is a closed curve which comes
back onto itself after making four loops, as shown in Fig.
9(a). The attractor for the driven chaotic oscillation,
shown in Fig. 9(b), does not come back onto itself. The
corresponding Poincaré maps are shown in Fig. 10. For
the 1:4 locked oscillation, the map consists of four points,
which are plotted as circles in Fig. 10(a). Figure 10(b)
shows the Poincaré map of the driven chaotic oscillation.
This Poincaré map is fuzzier than the Poincaré map
shown in Fig. 6(b) for the driven chaotic oscillation dis-
cussed in Sec. IV. The fuzzier Poincaré map in Fig. 10(b)
is indicative of a higher-dimensional attractor. In princi-
ple, one can extract the dimensionality of the attractor
from time-series data. However, for higher-dimensional
attractors, dimension measurements are easily corrupted
by experimental noise, and their interpretation is not
straightforward. For this work we feel that measure-
ments of the time-dependent spatial profiles are more
direct and robust.

Figure 11(a) shows the spatially dependent electric field
associated with the driven chaotic oscillation using the
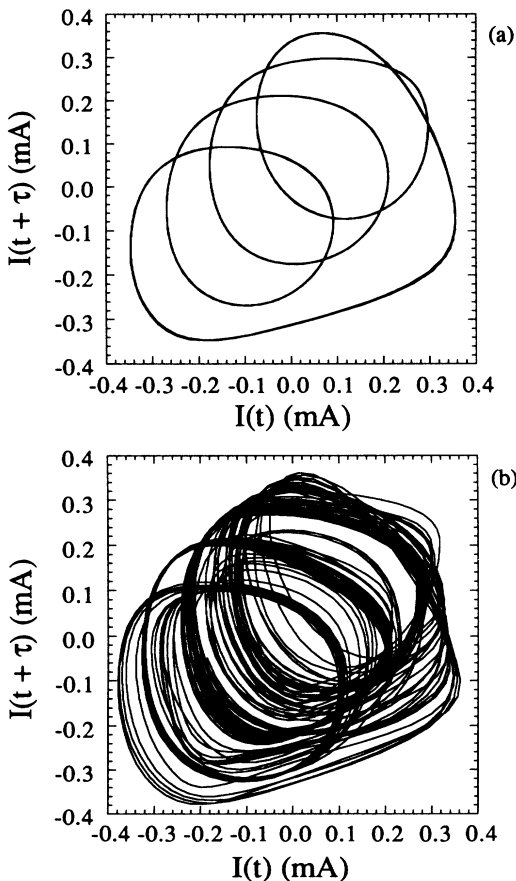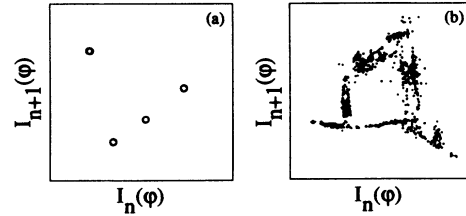same parameters as in Figs. 8(b), 9(b), and 10(b). The spa-

FIG. 10. Poincaré maps constructed by strobing the sample
current at a fixed phase of the ac drive and plotting as a map,
with $E_{dc} = 7.45$ V/cm and (a) the oscillation locked to the drive
with parameters $A = 1.63$ V/cm and $f_0/f_d = 0.19$; (b) the oscil-
lation driven chaotic with drive parameters $A = 1.91$ V/cm and
$f_0/f_d = 0.18$.

tial structure shown in Fig. 11(a) is much more compli-
cated than that of the spatially coherent chaotic oscilla-
tion shown in Fig. 7(a). In particular, Fig. 11(a) shows
that individual domains are nucleated and destroyed in
the bulk of the sample. At times there are multiple
domains in the sample. The bottom two traces in Fig.
11(a) show fluctuations in the local electric field at the
drive frequency before any domain is nucleated. The
next several traces show the growth and decay of larger
structures. Very few of the domains in Fig. 11(a) succeed
in reaching the last pair of capacitive probes, which is 1.6
mm from the receiving contact. The complex spatial
structure shown in Fig. 11(a) shows that, as suggested by
the Poincaré map in Fig. 10(b), for this set of drive pa-
rameters many degrees of freedom are important in the
system dynamics.

The corresponding correlation function $r(x = 1.6$
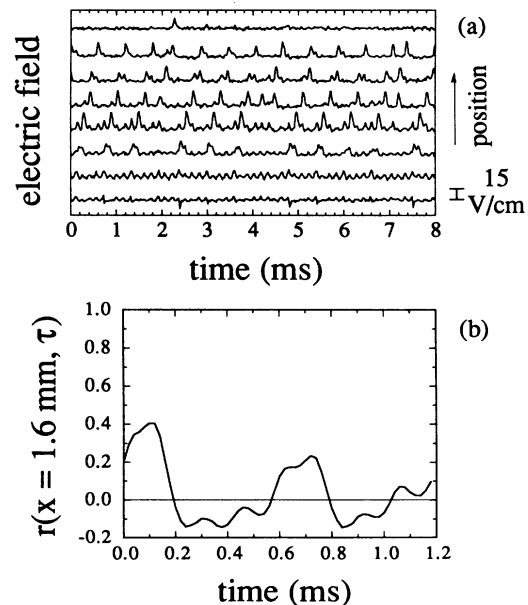mm,$\tau)$ for this driven chaotic oscillation is shown in Fig.

FIG. 9. Reconstructed attractors from sample current using
$\tau = 36$ μs with $E_{dc} = 7.45$ V/cm and (a) the oscillation locked to
the drive with parameters $A = 1.63$ V/cm and $f_0/f_d = 0.19$; (b)
the oscillation driven chaotic with drive parameters $A = 1.91$
V/cm and $f_0/f_d = 0.18$.

FIG. 11. Driven chaotic oscillation with $E_{dc} = 7.45$ V/cm,
$A = 1.91$ V/cm, and $f_0/f_d = 0.18$: (a) local sample electric field
vs time at eight equally spaced locations with the trace nearest
the injecting contact at the bottom; (b) $r(x = 1.6$ mm,$\tau)$ vs τ.
The horizontal line indicates $r(x = 1.6$ mm,$\tau) = 0$.

11(b). The height of the first peak is $r \approx 0.4$, as compared to $r \approx 0.7$ for the spatially coherent driven chaotic oscillation shown in Fig. 7. The first peak in Fig. 11(b) is smaller and broader than that in Fig. 7(b), because for Fig. 11(b) the sample electric field appears spatially incoherent. The first peak in r occurs at roughly the same time τ as in Fig. 7(b). This suggests that the domains move at approximately the same velocity as in the case of the spatially coherent oscillation. As in Fig. 7(b), there is a second peak in Fig. 11(b), occurring approximately one transit time after the first peak. The relative decay in height from the first peak to the second peak is 43% in Fig. 11(b) and 29% for the spatially coherent data in Fig. 7(b).

VI. THE EFFECT OF DRIVE PARAMETERS ON SPATIAL COHERENCE

In Secs. IV and V we demonstrated that we can observe spatial coherence or spatial incoherence when the oscillation is driven chaotic, depending on the drive parameters. In this section we map the dependence of spatial coherence on the drive parameters by measuring the spatially dependent electric field $E(x,t)$ for many different combinations of drive parameters. We use 16 different drive frequencies equally spaced in f_0/f_d, in the range $0.12 \leq f_0/f_d \leq 1$. At each drive frequency we measure $E(x,t)$ and compute the correlation function $r(x = 1.6 \text{ mm}, \tau)$ for each of 20 equally spaced amplitudes. Figure 12 is a plot of the measured values of r_{max}, the maximum value of the correlation function $r(x = 1.6 \text{ mm}, \tau)$ with respect to τ, for each set of drive parameters. This plot uses shading to indicate the value of r_{max}. The drive amplitude is on the vertical axis and f_0/f_d is on the horizontal axis. Note that the vertical axis extends over a much larger range in Fig. 12 than in Fig. 2 of Ref. 16 and that for most of the data shown in Fig. 12 we are driving the sample well above the critical line. The lighter regions in Fig. 12 correspond to drive parameters

for which the domain motion is spatially coherent and the darker regions correspond to less correlated behavior. The drive parameters used for Figs. 4(b), 5(b), 6(b), and 7 and those used for Figs. 8(b), 9(b), 10(b), and 11 are each indicated by dots in Fig. 12. As expected, the drive parameters used for Fig. 11 lie in a much darker region of Fig. 12 than do the parameters for Fig. 7.

The least correlated regions in Fig. 12 correspond to complex behavior, which occurs when the electric field variations due to the drive become comparable to domain sizes for the undriven oscillation. The darkest region in the upper left of Fig. 12 corresponds to drive parameters $A \approx 2$ V/cm and $f_0/f_d \approx 0.3$. This region of minimum correlation occurs when the drive period is approximately equal to a characteristic time $\Delta t \approx 0.3$ ms given by the domain velocity divided by the domain width. As discussed in Sec. I, the nucleation and destruction of domains is determined in part by the time-dependent electric field and charge-density profiles over a length scale slightly larger than a domain width. A high-field domain may nucleate when the electric field over a region becomes comparable to $E_c = 6.3$ V/cm, the threshold for spontaneous periodic oscillation for dc bias. Similarly, a high-field domain may be destroyed when the local electric field decreases sufficiently. Different regions of the sample are coupled by the fact that the spatial integral of the electric field over the entire sample is equal to the applied voltage at all times. This coupling results in complex behavior, as shown in Fig. 11(b). When A is sufficiently large $(A > E_{dc} - E_c)$, the time-dependent applied field swings below E_c and it becomes likely that the local sample electric field crosses thresholds for the nucleation and destruction of domains. For very large A, the ac drive destroys all domains before they reach the receiving contact. In this limit the correlation coefficient increases because the domains make relatively smaller contributions and the system behavior is dominated by the drive response. Above the critical line, the system displays hysteresis between several accessible states as the drive parameters are varied. Theoretical diagrams of accessible states for model systems above the critical line consist of complicated structures with islands. It is possible that some of the finer variations in correlation evident in Fig. 12 are associated with these structures.

Note that over intervals of the order of the transit time between probe pairs, the spatial coherence of the electric field for the driven oscillation is not strongly dependent on whether or not the oscillation is locked. The range of drive parameters in Fig. 12 includes regions in which the oscillation is frequency locked to the drive as well as regions of chaotic oscillations. Even when the spatial structure is complicated, domains move along the conduction direction with velocities close to the velocity of a domain for dc bias. The data in Fig. 12 are determined by the spatial coherence over times that are much shorter than the domain transit time. By contrast, the question of whether the oscillation is locked or chaotic can only be determined by examining a time series over a number of transit times.

Figure 13(a) shows an example of data for which the oscillation is temporally locked but spatially complex.
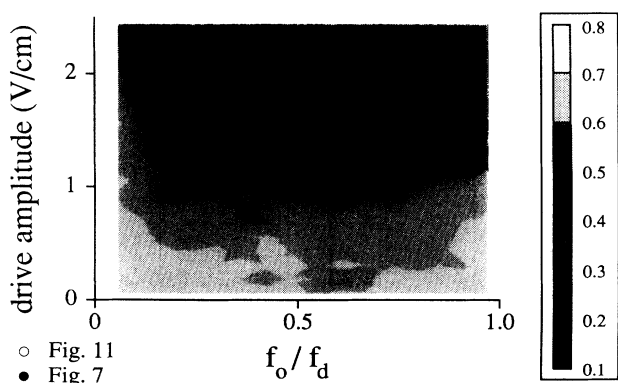

FIG. 12. Density plot of r_{max} constructed by measuring $E(x,t)$ on a grid of 18 drive frequencies and 20 drive amplitudes. The value of r_{max} is indicated by the shading. The black dot ($A = 0.85$ V/cm, $f_0/f_d = 0.62$) indicates the drive parameters used for the driven chaotic oscillation in Sec. IV and the white dot ($A = 1.91$ V/cm, $f_0/f_d = 0.18$) indicates the parameters used for the driven chaotic oscillation in Sec. V.
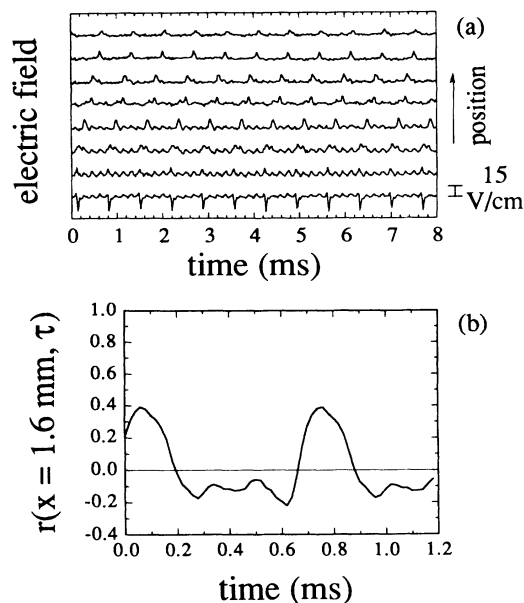
FIG. 13. 1:4 frequency-locked oscillation with $E_{dc} = 7.45$ V/cm, $A = 1.61$ V/cm, and $f_0/f_d = 0.21$: (a) local sample electric field vs time at eight equally spaced locations with the trace nearest the injecting contact at the bottom; (b) $r(x = 1.6$ mm,$\tau)$ vs τ. The horizontal line indicates $r(x = 1.6$ mm,$\tau) = 0$.

The figure shows the local sample electric field at successive positions as a function of time, with the bottom trace nearest to the injecting contact. The drive parameters are $f_0/f_d = 0.21$ and $A = 1.61$ V/cm, and the current oscillation is locked onto the drive in a 1:4 locking. This drive is sufficiently large that $E_{total}(t)$ swings below E_c. Because the oscillation is locked onto the drive, the local electric field at each position in the sample is periodic with a period equal to 0.7 ms, the shifted fundamental period of the oscillation. However, the time dependence of the local electric field varies considerably among the eight traces in Fig. 13. This is unlike the data shown in Figs. 1(c) and 2(c), for which $E_{total}(t) > E_c$ for all t, and a single domain with relatively constant shape moves through the sample. Near the injecting contact in Fig. 13, the electric field as a function of time has large fluctuations at the drive frequency. Closer to the receiving contact, these fluctuations are smaller and a high-field domain is observed at the fundamental oscillation frequency.

The corresponding correlation function $r(x = 1.6$ mm,$\tau)$ is shown in Fig. 13(b). The height of the first peak in the correlation function is approximately the same as that for the spatially incoherent chaotic data shown in Fig. 11(b). However, in Fig. 13(b), peaks in the correlation function $r(x = 1.6$ mm,$\tau)$ are periodic in τ, and the height of the second peak is equal to the height of the first peak because the oscillation is frequency locked.

As discussed above, the loss of spatial coherence occurs for an ac drive sufficiently large that $E_{total}(t)$ swings below $E_c = 6.3$ V/cm. In order to investigate the relation of this threshold field to the loss of spatial coherence, we measured the spatial coherence of the electric-
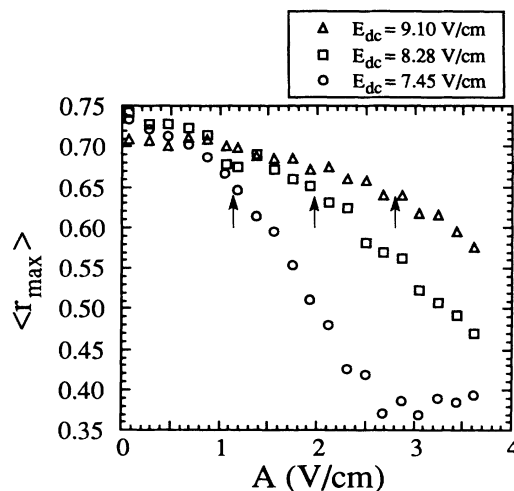

FIG. 14. $\langle r_{max} \rangle$ vs drive amplitude A for three different values of E_{dc}. The arrows indicate the value of A for which the minimum in applied electric field first decreases below $E_c = 6.3$ V/cm in each case.

field profiles for two dc bias fields E_{dc} above that used for Fig. 12. At each bias we measured $E(x,t)$ and computed $r(x = 1.6$ mm,$\tau)$ for the same grid of 20 equally spaced drive amplitudes and 16 drive frequencies equally spaced in f_0/f_d as used for Fig. 12. For each set of drive parameters, we determine r_{max}, the maximum amplitude of the correlation function $r(x = 1.6$ mm,$\tau)$ over the delay τ. We then average over f_0/f_d to determine the average maximum correlation amplitude $\langle r_{max} \rangle$ as a function of drive amplitude for each dc bias field, as shown in Fig. 14. The results for the bias field used for Fig. 12 are shown as circles and the results for the two higher bias fields are indicated by squares and triangles. For low drive amplitudes, the spatially dependent electric field is spatially coherent for all three of the bias fields and $\langle r_{max} \rangle$ is large in each case. As the ac drive amplitude is increased, a loss of spatial coherence occurs and $\langle r_{max} \rangle$ decreases. This decrease is fastest in the case of the smallest dc bias field and slowest for the largest bias field. This difference suggests that changes in the local electric field which result in the nucleation and destruction of domains in the bulk of the sample are more likely when the instantaneous applied electric field is close to E_c, the threshold for spontaneous periodic current oscillations.

VII. SUMMARY AND CONCLUSIONS

Driven space-charge domain motion in long samples of ultrapure Ge has been studied using an array of capacitive probes. Below the critical line for the occurrence of chaos, we observe frequency-locking behavior and an Arnold tongue diagram similar to that obtained by Gwinn and Westervelt.[4] Our spatially resolved measurements show that each period of the spontaneous oscillation is associated with the passage of a single space-charge domain through the sample. Frequency-locking initially occurs via smooth changes in the amplitude and motion of the domain rather than the production or destruction

of additional domains. The quasiperiodic transition to chaos is initially low dimensional in the sense that only a single domain is involved, in agreement with the success of the circle map in describing the temporal data of Gwinn and Westervelt.[4,13]

At larger drive amplitudes above the critical line, the motion becomes higher dimensional as domains are created and destroyed in the interior of the sample. Local formation and destruction of domains inside the sample depend on the local time-dependent profiles of electric field and trapped space charge, which both change continually in a driven sample in the postbreakdown regime. Different parts of the sample are coupled by the requirement that the spatial integral of the electric field equal the applied voltage, so that the formation of a high-field domain in one location tends to suppress the formation of domains in other locations, and may actually destroy other domains. In this regime the chaotic electric field profile becomes spatially complex as well as temporally chaotic.

ACKNOWLEDGMENTS

*Current address: Department of Physics, University of California, Santa Barbara, CA 93106.

[1]B. K. Ridley and R. G. Pratt, J. Phys. Chem. Solids **26**, 21 (1965).

[2]S. W. Teitsworth, R. M. Westervelt, and E. E. Haller, Phys. Rev. Lett. **51**, 825 (1983).

[3]J. Peinke, A. Mühlbach, R. P. Huebener, and J. Parisi, Phys. Lett. A **108**, 407 (1985).

[4]E. G. Gwinn and R. M. Westervelt, Phys. Rev. Lett. **57**, 1060 (1986); **59**, 247 (E) (1987).

[5]K. Aoki and K. Yamamoto, Phys. Lett. A **98**, 72 (1983).

[6]D. G. Seiler, C. L. Littler, R. J. Justice, and P. W. Milonni, Phys. Lett. A **108**, 462 (1985).

[7]K. Yamada, N. Takara, H. Imada, N. Miura, and C. Hamiguchi, Solid-State Electron. **31**, 809 (1988).

[8]B. K. Ridley, Proc. Phys. Soc. London **82**, 954 (1963).

[9]S. W. Teitsworth, Appl. Phys. A **48**, 127 (1989).

[10]V. V. Mitin, Appl. Phys. A **39**, 123 (1986).

[11]L. L. Bonilla and S. W. Teitsworth, Physica D **50**, 545 (1991).

[12]A. M. Kahn, D. J. Mar, and R. M. Westervelt, Phys. Rev. B **43**, 9740 (1991).

[13]E. G. Gwinn and R. M. Westervelt, Phys. Rev. Lett. **59**, 157 (1987).

[14]G. A. Held and C. Jeffries, Phys. Rev. Lett. **55**, 887 (1985).

[15]E. Mosekilde, R. Feldberg, C. Knudsen, and M. Hindsholm, Phys. Rev. B **41**, 2298 (1990).

[16]A. M. Kahn, D. J. Mar, and R. M. Westervelt, Phys. Rev. Lett. **68**, 369 (1992).

[17]A. M. Kahn, D. J. Mar, and R. M. Westervelt, Solid-State Electron. **32**, 1143 (1989).

[18]J. Peinke, J. Parisi, B. Röhricht, K. M. Mayer, U. Rau, W. Clauss, R. P. Huebener, G. Jungwirt, and W. Prettl, Appl. Phys. A **48**, 155 (1989), and references therein.

[19]P. Bak, T. Bohr, and M. H. Jensen, in *Directions in Chaos*, edited by B. L. Hao (World Scientific, Singapore, 1988), Vol. 2.

[20]W. H. Press, B. P. Flannery, S. A. Teukolsky, and W. T. Vetterling, *Numerical Recipes* (Cambridge University Press, New York, 1986).

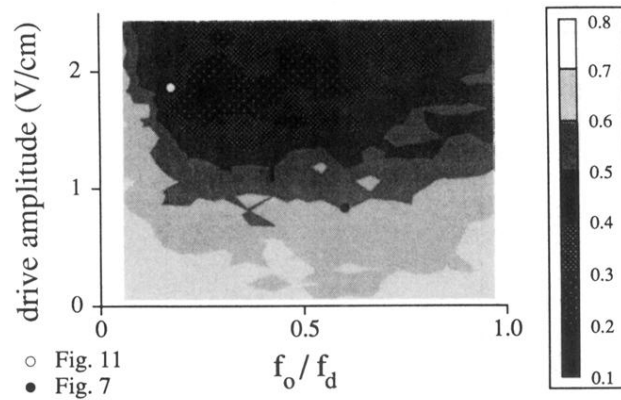[21]See, for example, H. G. Schuster, *Deterministic Chaos*, 2nd ed. (VCH, Weinheim, Germany, 1989).

FIG. 12. Density plot of r_{max} constructed by measuring $E(x,t)$ on a grid of 18 drive frequencies and 20 drive amplitudes. The value of r_{max} is indicated by the shading. The black dot ($A = 0.85$ V/cm, $f_0/f_d = 0.62$) indicates the drive parameters used for the driven chaotic oscillation in Sec. IV and the white dot ($A = 1.91$ V/cm, $f_0/f_d = 0.18$) indicates the parameters used for the driven chaotic oscillation in Sec. V.